

Molecular Systems Design & Engineering

Supplementary Information to:

An Energetics Assessment of Benzo[a]tetracene and Benzo[a]pyrene as Triplet-Triplet Annihilation Emitters

Xiaopeng Wang,^{*1} and Noa Marom^{2,3,4}

1, Qingdao Institute for Theoretical and Computational Sciences, Institute of Frontier and Interdisciplinary Science, Shandong University, Qingdao, Shandong 266237, P. R. China

2, Department of Materials Science and Engineering, Carnegie Mellon University, Pittsburgh, PA 15213, USA

3, Department of Physics, Carnegie Mellon University, Pittsburgh, PA 15213, USA

4, Department of Chemistry, Carnegie Mellon University, Pittsburgh, PA 15213, USA

*E-mail: 201999900092@sdu.edu.cn

CONTENTS

1. Excitation energies of known emitters
2. Excitation energies of alpha-sexithiophene (6T) under bond rotation
3. Frontier orbitals of phenanthrene
4. T_2 excited states of BA, BT, and BP

1. Excitation energies of known emitters

| No. | S ₁ (eV) | | | T ₁ (eV) | | |
|-----|---------------------|-------------------------|---------------------------------|---------------------|-------------------------|---------------------------------|
| | Calc. | Expt. | solvent | Calc. | Expt. | solvent |
| 1 | 3.21 | 3.31 ^[1] | n-heptane | 1.84 | 1.84 ^[2] | CHCl ₃ |
| 2 | 3.03 | 3.10 ^[3] | dimethylformamide | 1.70 | 1.82 ^[3] | dimethylformamide |
| 3 | 3.10 | 3.09 ^[4] | dimethylformamide | 1.77 | 1.77 ^[2] | CHCl ₃ |
| 4 | 2.44 | 2.66 ^[5] | acetonitrile | 1.29 | | |
| 5 | 2.37 | | | 1.23 | 1.20 ^[6,7] | N/A ^[a] |
| 6 | 2.80 | 2.81 ^[8] | methanol | 1.63 | | |
| 7 | 2.17 | 2.35 ^[9] | toluene | 1.00 | 1.14 ^[10] | N/A ^[b] |
| 8 | 3.67 | 3.65 ^[11] | CH ₂ Cl ₂ | 2.17 | 2.09 ^[12] | benzene |
| 9 | 3.52 | | | 2.08 | 2.09 ^[11,13] | CH ₂ Cl ₂ |
| 10 | 3.45 | 3.24 ^[14] | toluene | 2.07 | 1.95 ^[15] | cyclohexane |
| 11 | 2.79 | 2.81 ^[9] | toluene | 1.53 | 1.53 ^[9] | toluene |
| 12 | 2.65 | 2.83 ^[16,17] | dimethylformamide | 1.42 | | |
| 13 | 3.80 | 3.87 ^[18,19] | benzene | 2.51 | 2.48 ^[18,20] | benzene |
| 14 | 2.83 | 2.80 ^[10] | N/A ^[a] | 1.50 | 1.48 ^[10] | N/A ^[b] |
| 15 | 2.41 | 2.87 ^[21,22] | dioxane | 1.50 | | |

Table S1: Excitation energies calculated with TDDFT@B3LYP and extracted from experimental absorption spectra in solutions. ^[a] The solvents in experiments are not provided. ^[b] The energies are measured by energy transfer method.

Reference

- [1] J. Chem. Phys. 1949, 17, 470
- [2] Chem. Phys. Lett. 1968, 2, 671
- [3] J. Phys. Chem. A 2008, 112, 3906-3910
- [4] J. Phys. Chem. A 2009, 113, 1171
- [5] Chem. Phys. Lett. 1982, 92, 283
- [6] J. Org. Chem. 2011, 76, 7056-7064
- [7] J. Mater. Chem. C 2018, 6, 5785-5793

- [8] Chem. Commun. 2015, 51, 12403
- [9] New J. Phys. 2008, 10, 103002
- [10] J. Photochem. 1981, 16, 331-341
- [11] J. Phys. Chem. A 2006, 110, 11440-11445
- [12] Spectrochimica Acta, 1994, 50A, 1073-1079
- [13] RSC Adv. 2011, 1, 937-950
- [14] Dalton Trans. 2018, 47, 8557
- [15] Can. J. Chem. 1975, 53, 3269
- [16] J. Mater. Chem. C 2017, 5, 5063
- [17] Nature 2019, 565, 343
- [18] Phys. Chem. Chem. Phys. 2018, 20, 12182-12192
- [19] J. Phys. Chem. A 2009, 113, 5912-5917
- [20] Proc. R. Soc. London, Ser. A, 1972, 328, 457-479
- [21] J. Phys. Chem. 1995, 99, 9155-9159
- [22] J. Phys. Chem. 1996, 100, 18683-18695

2. Excitation energies of alpha-sexithiophene (6T) under bond rotation

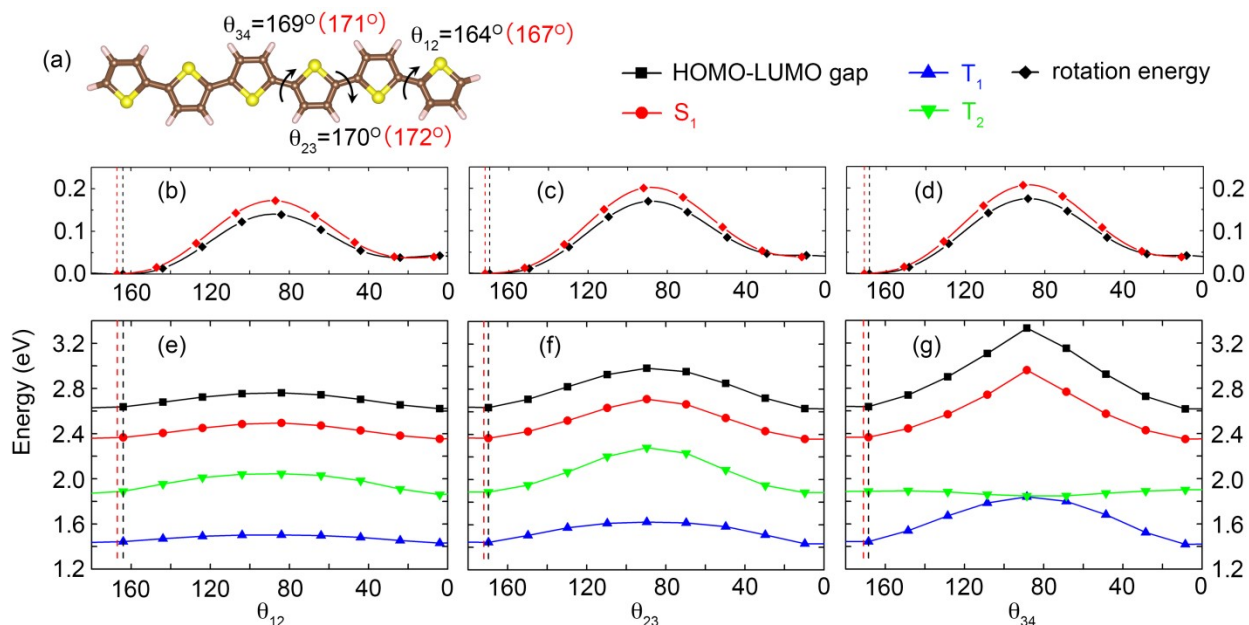


Figure S1: (a) Dihedral angles of optimized 6T. (b), (c), and (d) DFT@B3LYP rotation energies with (red) and without (black) a dispersion correction. The total energy of optimized 6T is referenced to zero. The vertical dash lines indicate optimal geometries in the ground state. The dihedral angles on the horizontal axis decrease from optimal values (about 170 deg) to planar (near 0 deg). (e), (f), and (g) DFT@B3LYP HOMO-LUMO gap and TDDFT@B3LYP S_1 , T_1 , and T_2 of 6T as a function of the dihedral angles θ_{12} , θ_{23} , and θ_{34} , respectively.

The modulation of the π -conjugation due to conformational changes in solution is simulated by rotating the S-C-C-S dihedral angles between the neighboring i^{th} and j^{th} thiophene rings in 6T, denoted as θ_{ij} . Figure S1(a) shows the dihedral angles in relaxed 6T, obtained with (red) and without (black) dispersion correction. To decouple the effect of rotating different bonds, only one torsion angle is rotated at a time with the others kept fixed at the relaxed values. Panels (b-d) in Figure S1 show the change in energy as a function of bond rotation. The energy barrier to rotation of one angle is less than 200 meV. In conjugated aromatic compounds, p_z molecular orbitals sharing the same nodal plane can form an extended π molecular orbital, resulting in a lower total energy. Therefore, when the thiophene rings in 6T are

approximately parallel or antiparallel to each other, the π molecular orbitals delocalize over the whole molecule, stabilizing it. This is reflected by the two local minima in the rotation energy curves. The minima are not at exactly 0 deg and 180 deg because of steric hindrance caused by repulsive interactions between neighboring thiophene rings. By the same token, an antiparallel alignment between neighboring thiophene rings, *i.e.* the optimal ground state geometry, is slightly more stable than a parallel configuration with close contacts between hydrogen atoms of neighboring rings.

Panels (e-g) in Figure S1 show the HOMO-LUMO gap and the S_1 , T_1 , and T_2 excitation energies of 6T as a function of θ_{ij} . The modulation of the π -conjugation due to bond rotations has a twofold effect on the HOMO-LUMO gap. First, as the three angles of 6T decrease from their equilibrium values to 90 deg, the HOMO-LUMO gap increases. Further rotation from 90 deg to a parallel alignment at 0 deg decreases the HOMO-LUMO gap. This is because the π conjugation between neighboring thiophene rings is hindered by a perpendicular orientation. Second, the HOMO-LUMO gap changes more dramatically with rotation of θ_{34} than of θ_{23} and hardly changes with rotation of θ_{12} . Rotation of one bond effectively divides the molecule into two segments. Going from the terminal bond (θ_{12}) toward the middle of the molecule (θ_{34}), the larger segment becomes shorter, causing a more significant decrease of the π -conjugation length, which has a greater impact on the HOMO-LUMO gap. The changes in S_1 and T_1 as a function of dihedral angles track the changes in the HOMO-LUMO gap. This is because S_1 and T_1 are dominated by the transition from HOMO to LUMO. In contrast, T_2 behaves differently. In particular, T_2 remains almost constant with the rotation of θ_{34} . This is because T_2 is dominated by other transitions.

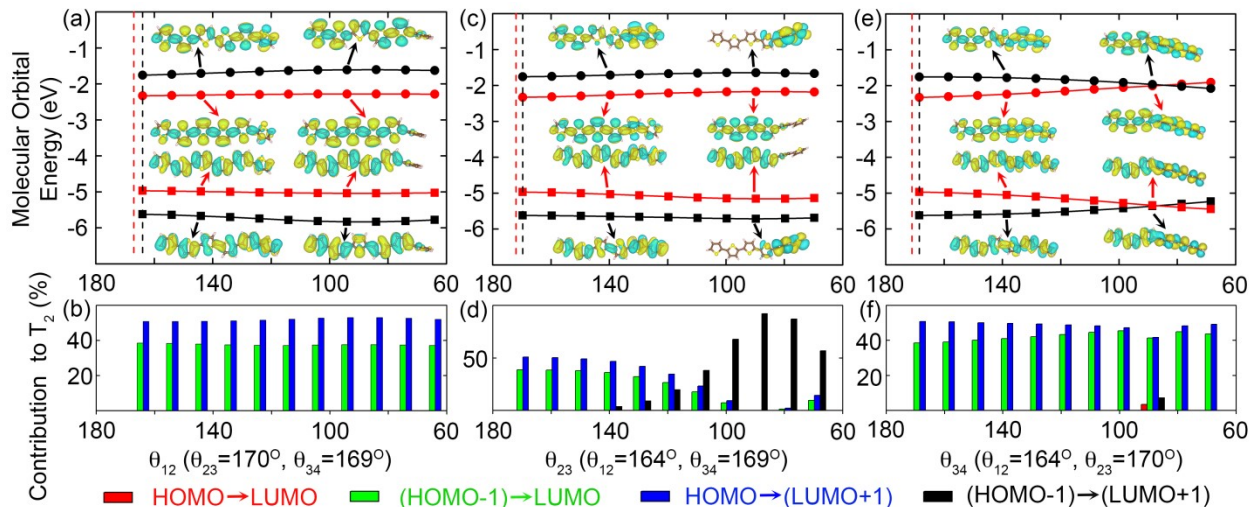


Figure S2: DFT@B3LYP molecular orbitals (HOMO-1 to LUMO+1) and orbital energies of 6T as a function of (a) θ_{12} , (c) θ_{23} , and (e) θ_{34} . Vertical dashed lines indicate the optimal ground state geometry. Breakdown of the transitions contributing to TDDFT@B3LYP T_2 of 6T as a function of (b) θ_{12} , (d) θ_{23} , and (f) θ_{34} .

Figure S2(a) shows the dependence of the HOMO, HOMO-1, LUMO, and LUMO+1 energies and the corresponding wave-functions on the dihedral angle θ_{12} . When θ_{12} rotates from its equilibrium position to 90 deg, 6T is effectively divided into two inequivalent segments, a larger segment of five thiophenes and a smaller segment of one. The corresponding wave-functions change significantly as all orbitals gradually become localized on the larger segment when the torsion angle reaches a perpendicular configuration. The energy gap between the occupied and virtual orbitals is increased slightly by the shortening of the π conjugation and the energy ordering of the molecular orbitals remains unchanged. Figure S2(b) shows that the contributions of the HOMO-1 to LUMO and HOMO to LUMO+1 transitions to T_2 does not change significantly with rotation of θ_{12} . The change in the T_2 energy seen in Figure S1(e) is caused by modulation of the energy gaps between the occupied and virtual orbitals involved in these two transitions.

Figure S2(c) shows the dependence of the HOMO, HOMO-1, LUMO, and LUMO+1 energies and the corresponding wave-functions on the dihedral angle θ_{23} .

When θ_{23} rotates to a perpendicular configuration the HOMO and LUMO reside on the larger segment of three thiophenes, whereas the HOMO-1 and LUMO+1 reside on the smaller segment of two thiophenes. Figure S2(d) shows that the change in orbital localization qualitatively alters the nature of T_2 . Initially, two transitions predominantly contribute to T_2 , HOMO-1 to LUMO and HOMO to LUMO+1. As θ_{23} approaches 90 deg, the occupied and virtual orbitals in each transition become localized on different segments. The spatial overlap between the occupied and virtual orbitals thus vanishes, hindering these two charge-transfer-like transitions and reducing their contributions to T_2 . At the same time, the occupied and virtual orbitals of another transition, HOMO-1 to LUMO+1, both become localized on the smaller segment, preserving their spatial overlap. As a result, the contribution of HOMO-1 to LUMO+1 to T_2 gradually increases, reaching more than 90% as θ_{23} approaches 90 deg. Thus, the T_2 energy increases with the rotation of θ_{23} to 90 deg for two reasons. First, the energy gap between the occupied and virtual orbitals increases. Second and more importantly, the two main transitions contributing to T_2 are replaced by a higher energy transition owing to orbital localization induced by bond rotation. In contrast, S_1 and T_1 are solely determined by the HOMO-LUMO gap. The HOMO and LUMO remain spatially localized on the same segment of the molecule. Therefore, there is no change in the transitions contributing to S_1 and T_1 with the rotation of θ_{23} .

Figure S2(e) shows the dependence of the HOMO, HOMO-1, LUMO, and LUMO+1 energies and the corresponding wave-functions on the dihedral angle θ_{34} . Rotation of θ_{34} divides the molecule into two identical segments, both consisting of 3 thiophene rings with the same dihedral angles. Consequently, the molecular orbitals remain delocalized over the whole molecule upon rotation of θ_{34} , such that the occupied and virtual molecular orbitals spatially overlap for all values of θ_{34} . As a result, the two transitions contributing to T_2 , HOMO-1 to LUMO and HOMO to

LUMO+1, do not change, as shown in Figure S2(f). The changes in the energies of S_1 , T_1 , and T_2 are only ascribed to molecular orbital energies. S_1 and T_1 increase with the HOMO-LUMO gap as θ_{34} rotates from its equilibrium position to 90 deg. The HOMO and LUMO+1 energies decrease similarly, whereas the HOMO-1 and LUMO energies increase similarly. Because the HOMO-(LUMO+1) and (HOMO-1)-LUMO gaps remain approximately constant, T_2 hardly changes with rotation of θ_{34} . When the orbital ordering changes, S_1 and T_1 are still dominated by HOMO to LUMO transitions, but between the new HOMO and LUMO. 6T has five rotatable inter-thiophene bonds, only one of which divides the molecule into two identical segments. Therefore, statistically, the overall effect of conformational flexibility is to increase T_2 in solution. All bond rotations increase S_1 and T_1 , which explains the discrepancy between the calculated and measured values in Figure 2 of the main text.

3. Frontier orbitals of phenanthrene

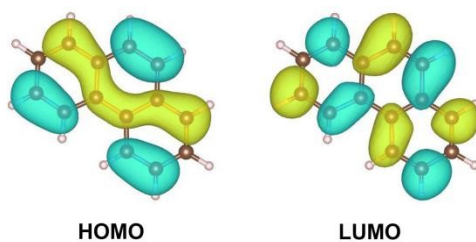


Figure S3: Visualization of DFT@B3LYP orbitals of phenanthrene.

Figure S3 shows the frontier orbitals of phenanthrene. They are not similar to those of BA, BT, and BP in Figure 4 of the main text.

4. T₂ excited states of BA, BT, and BP

| Transition | | BA | BT | BP |
|------------|--------|-------|-------|-------|
| From | To | | | |
| HOMO-2 | LUMO | 0 | 23.3% | 10.8% |
| HOMO-1 | LUMO | 34.4% | 27.0% | 42.0% |
| HOMO | LUMO+1 | 43.6% | 12.3% | 21.3% |
| HOMO | LUMO+2 | 0 | 22.0% | 15.8% |

Table S2: Transitions contributing to T₂ of BA, BT, and BP.

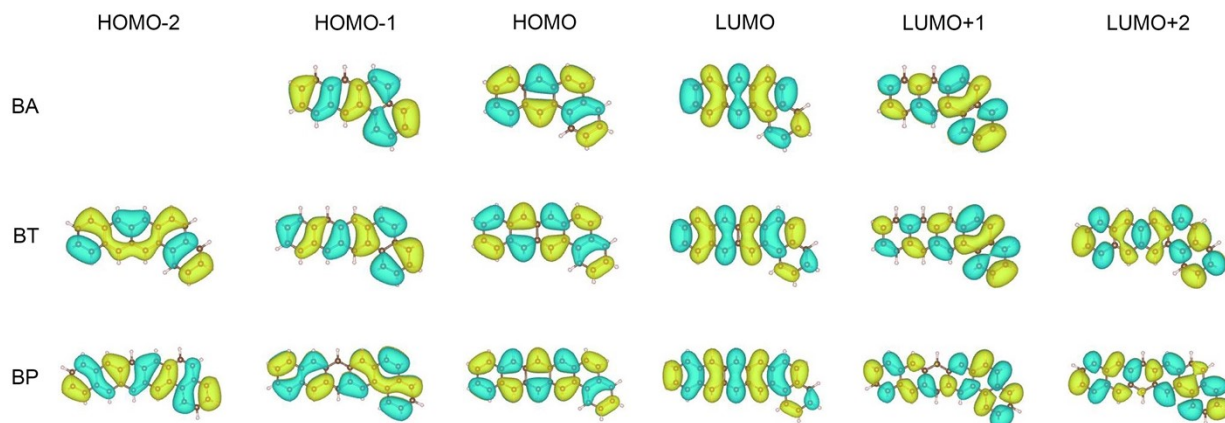


Figure S4: Visualization of DFT@B3LYP orbitals of BA, BT, and BP.

The spectral composition of T₂ for BA is different from BT and BP.